Output Formulation for Symmetrically Excited One-to-N Multimode Interference Coupler

Amir Hosseini, *Student Member, IEEE*, David Kwong, Che-Yun Lin, *Student Member, IEEE*, Beom Suk Lee, and Ray T. Chen, *Fellow, IEEE*

***Abstract*—In this paper, we present a closed form formulation for the output signals of one-to-N multimode interference coupler under symmetric excitation. We derive the output ports phases and show that the output phase has a quadratic dependence on the output port number. Using beam propagation simulations, we compare the analytical phase profile with the simulation results for different waveguiding structures. In the case of Si/SiO_2 structures, our formulation predicts the output phase profile with errors not more than about 1°. Finally, we show that nonideal effects, such as limited number of guided modes, modal phase errors, and extension of the field profile into the cladding layers have minimal effects on the phase profile in comparison with the output amplitudes. These results can be used in variety of optoelectronic applications, where the knowledge of the phase profile is crucial, such as optical phased arrays.**

***Index Terms*—Multimode interference (MMI) coupler, optical phased arrays, silicon photonics, waveguide theory.**

I. Introduction

MULTIMODE interference (MMI) based devices have been widely used in photonic integrated circuits (PICs) as compact-size passive power splitters [1], [2], 90° hybrid couplers [3], and mode-matching stages [4]. MMI-based active devices such as optical switches [5], [6] and phased-array multiplexers [7] have been theoretically studied and experimentally demonstrated. The interest in MMI-based devices stems from properties, such as compact size, low power imbalance, stable power splitting ratio, low cross talk, large optical bandwidth, and high tolerance to fabrication process errors [2], [8], which render such devices suitable for integration in PICs with complex passive networks including power splitters and signal routing. Compared to Y-branches, MMI splitters are smaller and benefit from scalability as the number of the output ports grow large.

Several studies investigated the quality of the output signals in MMI couplers based on power uniformity [3], [9] and image resolution [10]. Also, several techniques have been proposed to improve the signal quality, such as tapered multimode waveguide [11], graded-index waveguides [12], and deeply etched air trenches at the boundary of the multimode section [2].

Manuscript received May 6, 2009; revised August 24, 2009. First published October 20, 2009; current version published February 5, 2010. This research is supported by the Multidisciplinary University Research Initiative program through the Air Force Office of Scientific Research, USA.

The authors are with the Department of Electrical and Computer Engineering, Microelectronics Research Center, University of Texas at Austin, Austin, TX 78758 USA (e-mail: ahoss@ece.utexas.edu; diddykwong@gmail.com; cheyunlin@gmail.com; bslee74@gmail.com; chen@ece.utexas.edu).

Color versions of one or more of the figures in this paper are available online at http://ieeexplore.ieee.org.

Digital Object Identifier 10.1109/JSTQE.2009.2032669

In addition to being used as power splitters, MMI couplers can be also used in more complex photonic components, where the phase of the output signal is also important, such as 90° hybrid couplers [3] and in high-speed phased-array optical beam steerers [13]. Despite the effort in investigating the power profile at the MMI output ports, the studies of phase profile are much more limited. Bachmann *et al.* [14] presented general phase relations derived for $N \times N$ MMI couplers, based on the assumption of the superposition of self-images of equal amplitudes.

In general, the knowledge of the MMI output phase profile is essential, when the phase differences between the signals of different output arms determine the performance of the compact optoelectronic devices that employ a multimode waveguide region to generate several channels, such as optical spatial quantized analog-to-digital converters [15], optical beam steerers [13], and phased-arrayed photonic switches [16]. For example, generalizing a two-channel optical switch based on the phased-array optical beam steering [13] to more than two channel systems is not possible without necessary compensation of the MMI output phase profile.

Symmetrically excited $1 \times N$ MMI couplers are the most commonly used power splitters in photonic circuitries, where the number of output ports has been reported from 2 to as large as 64 [17]. In this paper, starting from the field profile at the MMI coupler input, we derive the complex field profile at N-fold imaging length for symmetrically excited $1 \times N$ MMIs, without the assumptions of N-fold image superposition at the output. The equal power distribution in the ideal case assumed here, where the phase errors at imaging lengths are neglected, is a result of our derivations. Analytical expressions for the output phases are presented based on the derived complex output field profile. Our results confirm the general phase relations predicted in [14] for the case of symmetrically excited $1 \times N$ MMI couplers. We compare the results with the beam propagation simulations and examine the source of the output phase errors with respect to the analytical model. Our analysis is most accurate for high-index contrast waveguides. However, image enhancing techniques, such as etched air trenches introduced to define the edges of the MMI coupler [2], make the presented analysis applicable to low-index contrast waveguides, such as polymer-based structures. Finally, we discuss the effect of this technique on the output phase profile, which determine the controllability of the output phased array.

II. MMI Couplers

Self-imaging is a phenomenon in multimode waveguides by which an input field profile is reproduced in single or multiple

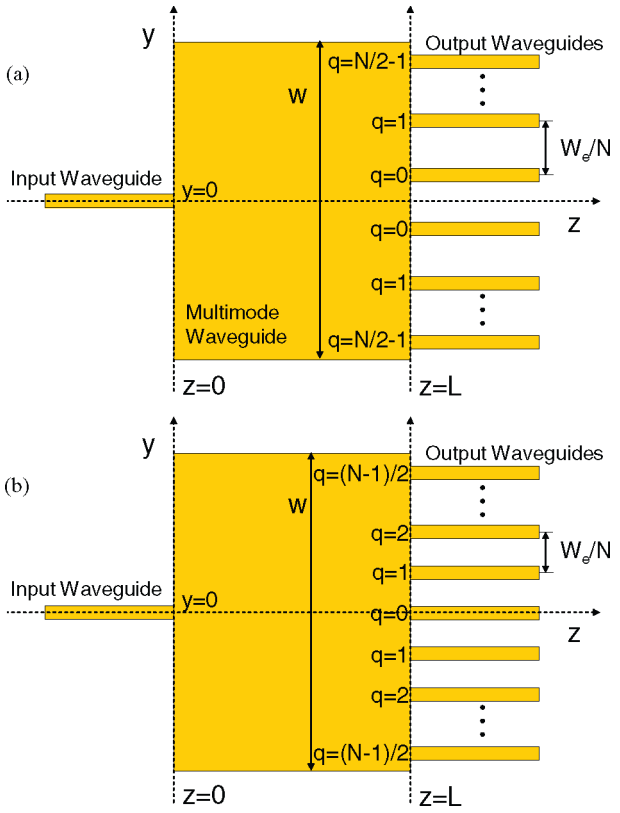

Fig. 1. Schematics of $1 \times N$ symmetric MMI coupler: (a) even N and (b) odd N.

images at periodic intervals along the propagation direction of the guide [3]. This effect has been exploited in different MMI-based structures. Several MMI coupler structures have been theoretically studied and experimentally demonstrated [1]–[3], [9], [10], and [17]. In Fig. 1, the multimode waveguide section consists of a W-wide core of refractive index n_c, embedded in between cladding layers of n_0. In the case of 3-D waveguides, an equivalent 2-D representation can be made by techniques such as the effective index method or the spectral index method [3]. The multimode section can support maximum $M+1$ number of modes. For each mode p, the dispersion relation is given as

$$\beta_p^2 + \kappa_{yp}^2 = \left(\frac{2\pi n_c}{\lambda_0}\right)^2 \tag{1}$$

where β_p is the propagation constant of the pth mode, λ_0 is a free-space wavelength, and κ_{yp} is the lateral wavenumber of the pth mode, given as $\kappa_{yp} = (p+1)\pi/W_e$, where W_e is the effective width for mode m including the penetration depth due to the Goose–Hahnchen shift [2]. The propagation constant β_p can be approximated as

$$\beta_p \simeq \beta_0 - \frac{p(p+2)\pi}{3L_\pi} \tag{2}$$

where $L_\pi = \pi/(\beta_0 - \beta_1) \approx 4n_c W_e^2/3\lambda_0$ [3]. Given the orthogonality of the propagating modes, any input field profile at $z=0$ can be written as a linear combination of the propagating modes

$$\Phi(y, Z=0) = \sum_{p=0}^{M} c_p \phi_p(y) \tag{3}$$

where c_p is the excitation coefficient of the pth mode by the given input field profile calculated as the overlap integrals of the pth mode and the input field profile [3]. Each excited mode accumulates phase shifts according to its own propagation constant, and therefore, the field profile at any $z=L$ can be represented by

$$\exp(-j\beta_0 L)\sum_{p=0}^{M} c_p\phi_p(y)\exp(-j(\beta_p-\beta_0)L)$$

$$\approx \exp(-j\beta_0 L)\sum_{p=0}^{M} c_p\phi_p(y)\exp\left(j\frac{p(p+2)\pi}{3L_\pi}L\right). \tag{4}$$

At $L = 3rL_\pi$ with $r = 1, 2, \ldots$, all the exponential terms in (4) become in-phase with one another and a single image of the input field profile is formed. Generally, an N-fold image of the input field profile is formed at $L = 3L_\pi/N$. In the case of symmetric excitation, $\Phi(-y, Z=0) = \Phi(y, Z=0)$, only the even modes $p = 2m$, $m \in \mathbb{Z}$ are excited. We will use this fact in Section III to simplify the field expression at the imaging lengths. This type of excitation can be realized by a symmetric input field profile fed to the center of the multimode waveguide as demonstrated by Fig. 1. This has been known to result in short $1 \times N$ couplers, where N is the number of output ports [3]. The required length for such a coupler is given as $L = 3rL_\pi/4N$, which is four times shorter than the general case.

In the case of $1 \times N$ couplers, the output power is ideally designed to be equally divided among the output ports, and therefore, the field amplitude at the output ports is $1/\sqrt{N}$. In reality, however, the approximation in (2) becomes inaccurate, especially for the higher order modes in low-refractive-index contrast waveguides. Therefore, the Goose–Hahnchen effect becomes mode dependent and the accumulated phase shift of each mode is different from the ideal case by an error of

$$\Delta\psi_p \approx \frac{\lambda_0^2(p+1)^4\pi}{2Nn_c^2W_{\text{eff}}^2}\left[\frac{1}{8} - \frac{\lambda_0 n_c^2}{6\pi W_e(n_c^2 - n_0^2)^{1.5}}\right] \tag{5}$$

for the N-fold imaging length $L = 3rL_\pi/N$ [9]. The existence of these modal phase errors is inherent in the dispersion law of the dielectric slab waveguides. Additional phase errors occur, when the observation plane is shifted away from the paraxial plane [10]. In the case of the symmetric excitation, the accumulated phase error at the N-fold imaging length is $\Delta\psi_p/4$. This error would result in nonuniformity in the output power distribution. In the next section, we derive a closed form formula for the output field profile.

III. Symmetric MMI Coupler Output Phase Profile

Consider the $1 \times N$ MMI coupler shown in Fig. 1. In order to analyze the output properties, such as image resolution, contrast, etc., Ulrich and Kamiya approximated the multimode waveguide propagating modes field profiles with cosine

functions

$$\phi_p(y) = \cos \kappa_{yp} y \tag{6}$$

which allowed them to apply the Fourier transform properties to the field presentation in [10]. We adopt the same technique to take the position (in the y-direction) of the images formed into account. In general, nonspurious radiation modes as well as other discrete modes should be considered to fully satisfy the energy conservation law in the vicinity of discontinuity [18]. In our analysis, we ignore such modes for simplicity.

Consider one of the N images of the input field at an N-fold imaging length and shifted in the y-direction to $y = y_q$. Based on (3), this image can be presented as $B\phi(y - y_q, z = 0) = B\sum_{p=0}^{M} c_p \phi_p(y - y_q)$, where $B = e^{j\theta_q}/\sqrt{N}$, assuming uniform power distribution. θ_q is the phase shift at ports that correspond to q in Fig. 1 with respect to the input signal at $z = 0$. Our goal is to derive an analytical expression for the θ_q value. Note that the assumption of N-fold image formation and uniform power distribution in the case of symmetric MMI coupler intuitively bridge the derivations in the Appendixes A and B to the analytical expressions of the total field profile at $L = 3rL_\pi/N$. However, such assumptions are not crucial at this point but are the results of the derivations. As shown in Fig. 1(a) and (b) for the N images formed at the output ports the lateral shifts of the position with respect to the input image are $y_q = \pm W_e/2N, \pm 3W_e/2N, \ldots, \pm(N-1)W_e/2N$, for even N, and $y_q = 0, \pm W_e/N, \pm 2W_e/N, \pm(N-1)W_e/2N$, for odd N. Therefore, at an N-fold imaging length (L_0) the field profile $\Phi(y, L_0)$ is

$$\frac{1}{\sqrt{N}} \sum_{q=0}^{N/2-1} \exp(j\theta_q) \sum_{p=0}^{M} c_p \left\{ \cos\left[\kappa_{y(p)}\left(y - \frac{(2q+1)W_e}{2N}\right)\right] + \cos\left[\kappa_{yp}\left(y + \frac{(2q+1)W_e}{2N}\right)\right]\right\} \tag{7}$$

for even N, and

$$\frac{1}{\sqrt{N}} \exp(j\theta_0) + \frac{1}{\sqrt{N}} \sum_{q=0}^{(N-1)/2} \exp(j\theta_q) \times \sum_{p=0}^{M} c_p \left\{ \cos\left[\kappa_{y(p)}\left(y - \frac{qW_e}{N}\right)\right] + \cos\left[\kappa_{yp}\left(y + \frac{qW_e}{N}\right)\right]\right\} \tag{8}$$

for odd N. In (7) and (8), the symmetry of the structure have been taken into account by letting $\theta_{-q} = \theta_q$. We can simplify (7) and (8), using the trigonometric identity $\cos(a \pm b) = \cos(a)\cos(b) \mp \sin(a)\sin(b)$. We also noted that when the multimode waveguide is symmetrically excited, only the even modes of the multimode region are excited, and therefore, $c_p = 0$, for odd p values. Using $\kappa_{y(p)} y = \kappa_{y(2m)} y = ((2m+1)/W_e)\pi$, we can rewrite (7) and (8) with $c_p = c_{2m}$

$$\frac{2}{\sqrt{N}} \sum_{q=0}^{N/2-1} \exp(j\theta_q) \times \sum_{m=0}^{M/2} c_{2m} \cos(\kappa_{y(2m)} y) \cos\left[\frac{(2m+1)(2q+1)}{2N}\pi\right] \tag{9}$$

for even N, and

$$\frac{1}{\sqrt{N}} \exp(j\theta_0) + \frac{2}{\sqrt{N}} \sum_{q=0}^{(N-1)/2} \exp(j\theta_q) \times \sum_{m=0}^{M/2} c_{2m} \cos(\kappa_{y(2m)} y) \cos\left[\frac{(2m+1)q}{N}\pi\right] \tag{10}$$

for odd N. Note that M is even, and thus, $M/2$ is an integer. We can also rewrite the field profile from (4) at a symmetric N-fold imaging length, $L_0 = 3L_\pi/4N$, considering $p = 2m$

$$\Phi(y, L_0) = \sum_{m=0}^{M/2} c_{2m}\, \phi_{2m}(y) \exp\left(j\frac{m(m+1)\pi}{N}\right). \tag{11}$$

Note that we have dropped the common factor $\exp(-j\beta_0 L_0)$ for simplicity, but we will add it back later. In the Appendix A, we have proved that in the case of even N

$$\sum_{m=0}^{M/2} c_{2m}\, \phi_{2m}(y) \exp\left(\frac{jm(m+1)}{N}\pi\right) = \frac{2e^{j((N-2)/4N)\pi}}{\sqrt{N}} \sum_{m=0}^{M/2} c_{2m}\, \phi_{2m}(y) \times \sum_{q=0}^{(N/2)-1} \exp\left(-j\frac{q(q+1)}{N}\pi\right) \cos\left(\frac{(2m+1)(2q+1)\pi}{2N}\right). \tag{12}$$

Comparing (12) and (9), one can conclude that

$$\exp(j\theta_q) = \exp\left(j\frac{N-2}{4N}\pi\right) \times \exp\left(-j\frac{q(q+1)}{N}\pi\right). \tag{13}$$

Taking the common factor, $\exp(-j\beta_0 L_0)$, into account

$$\theta_q = -\beta_0 L_0 + \frac{N - 2 - 4q(q+1)}{4N}\pi \tag{14}$$

for $q = 0, 1, \ldots, N/2 - 1$, where q is assigned to the output ports as shown in Fig. 1(a). Note that the phase profile is symmetric with respect to the line $y = 0$. We can identify that the phase profile has a propagation accumulated phase term, a constant term depending on the number of output channels, which is the same for all the channels, and a term that quadratically depends on the channel number (starting from the middle of the waveguide).

In the case of odd N, one can show (see Appendix B)

$$\sum_{m=0}^{M/2} c_{2m}\,\phi_{tm}(y)\exp\left(j\frac{m(m+1)}{N}\pi\right) = \frac{e^{j((N-1)/4N)\pi}}{\sqrt{N}}\sum_{m=0}^{M/2} c_{2m}\,\phi_{2m}(y) \times\left(1+2\sum_{q=1}^{(N-1)/2}\exp\left(-j\frac{q^2}{N}\pi\right)\cos\left(\frac{2m+1}{N}q\pi\right)\right). \tag{15}$$

Similarly, in the case of odd N, comparing (15) and (10), one can conclude that

$$\theta_q = -\beta_0 L_0 + \frac{N-1-4q^2}{4N}\pi \tag{16}$$

for $q = 0, 1, \ldots, (N-1)/2$, where the q values are assigned to the output ports as shown in Fig. 1(b). Again, the phase profile is symmetric with respect to the line $y = 0$. Equations (14) and (16) confirm the general phase relations predicted in [14] for the case of symmetrically excited $1 \times N$ MMI couplers.

IV. Simulation Results and Discussion

In order to investigate the MMI structure output phase, we performed 3-D semivectorial beam propagation method (SVBPM) simulations using the BeamPROP module in RSoft CAD. In the beam propagation method, the field expression is separated into a slow-varying envelop and a fast-varying phase term. It is also assumed that the propagation is primarily along the propagation direction (z-direction). Since boundary conditions of x or y polarization can be incorporated into the finite-difference equation, BPM can be semivectorial [19]. SVBPM simulators can be implemented to reduce the computational expenses when compared to full-field simulators, such as finite-difference time domain. However, BPM simulations cannot handle beams propagating at a large angle to the z-axis or backward reflections. In the case of the MMI structures in this paper, we are neither concerned about the backward reflections nor wide angle propagations, thus, we can use SVBPM to find the output phase profile.

Fig. 2(a) shows the field propagation profile of a 1×6 Si/SiO_2 MMI coupler. The refractive indexes of the core and the cladding layers are $n_c = n_{\mathrm{Si}} = 3.47$ and $n_0 = n_{\mathrm{SiO_2}} = 1.45$, respectively. A cross section diagram of the multimode waveguide is shown in the inset of Fig. 2(c). The input and output ports consist of waveguides with 2.5 μm $\times\, h$ cross sections, where $h = 0.25$ μm is the thickness of the multimode waveguide [see Fig. 2(c) inset]. In order to compare the BPM simulation results with the analytical formula derived in the Section III, we take one of the middle output ports (for even N) [port number 3 in Fig. 2(a)] to be the phase reference, for which the phase is set to zero. Fig. 2(c) compares the output phase profile from the BPM simulations with that calculated using (14).

Note that the high core/cladding layers refractive index contrast in the Si/SiO_2 MMI coupler results in well-defined edges

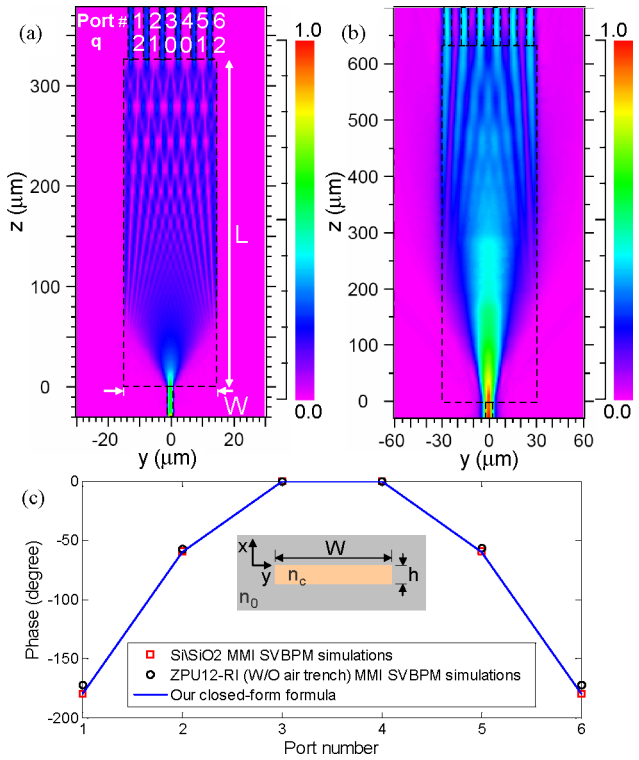

Fig. 2. Beam propagation simulation results. (a) Field propagation profile at $x = 0$, for the Si/SiO_2 MMI with $N = 6$, $W = 30$ μm, $L = 325$ μm, and $h = 0.25$ μm. (b) Field propagation profile at $x = 0$, for the ZPU12-RI MMI with $N = 6, W = 60$ μm, $L = 625$ μm, and $h = 5$ μm. (c) Phase profile from BPM simulation of the MMI structures in (a) and (b) and the ideal phase profile form the analytical model with q values shown in (a). A cross section diagram of the multimode waveguide is shown in the inset of (c).

along the length of the multimode waveguide. In order to examine the sources of the phase errors and to investigate the validity of the analytical model for phase profile in the case of low-refractive-index contrast, we simulated a polymer waveguide structure composed of ZPU12-RI series polymer materials from ChemOptics [2], where the core and the cladding layers are ZPU12-460 ($n_c = 1.46$) and (ZPU12-450) ($n_0 = 1.45$), respectively. For this MMI structure, input and output waveguides of 5 μm $\times\, h$ cross section and $h = 5$ μm are assumed. This MMI structure is adopted from [2] with no air trench along the multimode waveguide. Fig. 2(b) shows the field propagation profile of the ZPU12-RI MMI coupler and Fig. 2(c) compares the simulated output phase profile with the analytical calculations derived in Section III.

Table I compares the BPM simulation results with the analytical calculations for several Si/SiO_2 and ZPU12-RI MMIs with the number of output ports varying from $N = 3$ to 12. In the case of Si/SiO_2 MMIs, the MMI width $W = N \times 5$ μm and the MMI height $h = 0.25$ μm. In the case of the ZPU12-RI MMIs, $W = N \times 10$ μm and $h = 5$ μm. In all cases, the MMI length is $L = 3L_\pi/4N$, and the input waveguide is excited by a TE-polarized mode. $\lambda_0 = 1600$ nm and $\Delta x = \Delta y = \Delta z = \lambda_0/20n_{\mathrm{core}}$. The output ports that correspond to $q = 0$ are taken as the reference, for which the phase is zero ($\theta_0 = 0$). According to Fig. 1, for the middle output port in the case of odd N values

TABLE I
CLOSED-FORM ANALYTICAL FORMULATION RESULTS VERSUS BPM SIMULATIONS

		Analytical Model									
Analytical Model	θ_j	N=3	N=4	N=5	N=6	N=7	N=8	N=9	N=10	N=11	N=12
	θ_0	0	0	0	0	0	0	0	0	0	0
	θ_1	-60	-90	-36	-60	-25.7	-45	-20	-36	-16.4	-30
	θ_2	x	x	-144	-180	-102.9	-135	-80	-108	-65.5	-90
	θ_3	x	x	x	x	-231.4	-270	-180	-216	-147.3	-180
	θ_4	x	x	x	x	x	x	-320	-360	-261.8	-300
	θ_5	x	x	x	x	x	x	x	x	-409.1	-450
		BPM Simulation									
Si/SiO$_2$	θ_j	N=3	N=4	N=5	N=6	N=7	N=8	N=9	N=10	N=11	N=12
	θ_0	0	0	0	0	0	0	0	0	0	0
	θ_1	-58.8	-89.1	-36.6	-59.5	-25.5	-44.4	-19.8	-35.4	-16.4	-30.0
	θ_2	x	x	-144.7	-179.7	-102.3	-134.1	-79.7	-107.7	-64.5	-90.1
	θ_3	x	x	x	x	-230.7	-270.0	-179.6	-215.5	-146.9	-180.3
	θ_4	x	x	x	x	x	x	-319.1	-359.2	-261.3	-299.9
	θ_5	x	x	x	x	x	x	x	x	-408.5	-449.6
		BPM Simulation									
ZPU12-RI (W/O Air Trench)	θ_j	N=3	N=4	N=5	N=6	N=7	N=8	N=9	N=10	N=11	N=12
	θ_0	0	0	0	0	0	0	0	0	0	0
	θ_1	-55.9	-84.8	-34.7	-57.1	-25.3	-44.1	-19.7	-35.8	-16.1	-29.6
	θ_2	x	x	-138.6	-172.3	-100.7	-131.3	-79.6	-105.6	-64.6	-89.5
	θ_3	x	x	x	x	-225.3	-261.4	-176.1	-209.8	-144.6	-177.3
	θ_4	x	x	x	x	x	x	-312.8	-349.4	-254.8	-293.5
	θ_5	x	x	x	x	x	x	x	x	-399.9	-442.3
		BPM Simulation									
ZPU12-RI (W/ Air Trench)	θ_j	N=3	N=4	N=5	N=6	N=7	N=8	N=9	N=10	N=11	N=12
	θ_0	0	0	0	0	0	0	0	0	0	0
	θ_1	-57.4	-87.0	-35.3	-57.1	-25.4	-43.1	-19.7	-35.7	-16.5	-29.9
	θ_2	x	x	-142.2	-176.5	-101.0	-132.2	-79.8	-108.5	-65.9	-89.8
	θ_3	x	x	x	x	-227.8	-266.2	-179.7	-215.1	-148.0	-179.5
	θ_4	x	x	x	x	x	x	-317.8	-359.0	-262.3	-299.1
	θ_5	x	x	x	x	x	x	x	x	-407.0	-448.6

All the numbers are in degree.

and for the two equivalent output ports in the middle in the case of even N values q is 0.

In the case of the Si/SiO$_2$ MMIs, the output phase values are within about 1° of the calculated values from the analytical models in (14) and (16). In the case of the ZPU12-RI MMIs, the average phase profile error with respect to the analytical models is about 5°. This error can be attributed to modal phase errors expressed in (5), and also the deviation of the modal field profiles $[\phi_p(y)]$ from the cosine-shape functions as the penetration of the evanescent field into the cladding layers is more in lower refractive index contrast waveguides. The modal phase errors are the main cause of nonuniformity in the output amplitudes [9], [10]. Table I indicates that the output phase deviates more from the ideal self-imaging guide analytical model as the output port is shifted away from the paraxial plane ($y = 0$). Therefore, the main source of errors in the phase profile is the deviation of the modal field profiles from the cosine-shape functions. In fact, for large N, the output phase values for the ports in the middle of the MMI structure are almost the same as those in the Si/SiO$_2$ MMIs and ZPU12-RI MMIs.

Wang and Chen showed that etching deep air trenches along the multimode waveguide to define the edges of the MMI coupler substantially reduced the lateral penetration depth into the cladding in the case of low-contrast refractive index structures [2]. Therefore, the effective width of all the guided modes is approximately the same as the actual width of the MMI coupler. Hence, the presence of air trenches improves image quality. In order to investigate the effect of the such air trenches on the output phase profile, we simulated the same ZPU12-RI MMI structures but with air trenches along the multimode waveguide sides. The resulted output phase values are presented in Table I. Introducing the air trenches specially improves the modal field profiles away from the paraxial plane, and therefore, correction in the output phase values is more significant in the outer ports (large q) compared to that of the ports in the middle (small q) of the MMI structure.

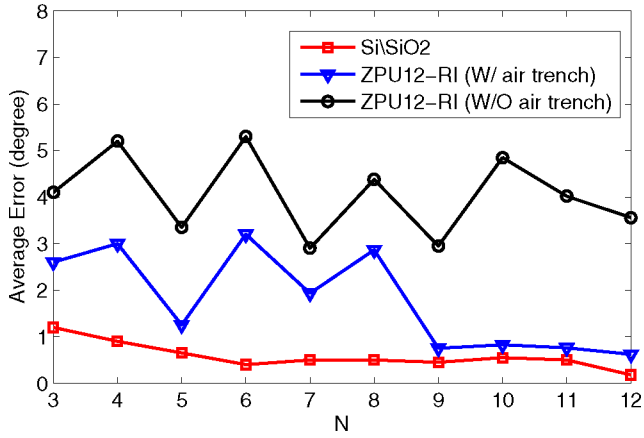

Fig. 3. The average output phase profile error of the Si/SiO$_2$ MMIs, ZPU12-RI MMIs without air trenches and ZPU12-RI MMIs with air trenches with respect to the analytical model.

Fig. 3 illustrates the average output phase error of the Si/SiO$_2$ MMIs, ZPU12-RI MMIs without air trenches and ZPU12-RI MMIs with air trenches with respect to the analytical model as the number of outputs changes from $N = 3$ to 12. In the

case of the PU12-RI MMIs with air trenches, the output phase of the middle ports are close to the ideal values at large N values, similar to that of the PU12-RI MMIs with air trenches. Therefore, the correction of the output phase of the outer ports by introducing the air trench, results in a smaller average output phase profile error as the N increases.

V. Conclusion

We derive analytical formulations for the output phase profile of symmetrically excited one-to-N MMI couplers. The output phase increases quadratically from the middle of the MMI waveguide, which needs to be taken into account for phase-dependent applications, such as optical phased arrays. We compare the analytical calculations with the results of beam propagation simulations for different MMI structures and find that the effect of the penetration of the field into the cladding layers at the side walls is more than the modal phase errors on the output phase profile. However, even in the case of low-refractive-index contrast of $\Delta n = 0.01$, the output phase values are within the 10° intervals from the predicted values.

Appendix A
Proof for Even N

In the case of $N = 2K$, $K \in \mathbb{Z}$, we need to show

$$\frac{2e^{j((N-2)/4N)\pi}}{\sqrt{N}} \sum_{m=0}^{M/2} C_{2m}\phi_{2m}(y) \times \sum_{q=0}^{(N/2)-1} \exp\left(-j\frac{q(q+1)}{N}\pi\right)\cos\left(\frac{(2m+1)(2q+1)\pi}{2N}\right) = \sum_{m=0}^{M/2} C_{2m}\phi_{2m}(y)\exp\left(\frac{jm(m+1)}{N}\pi\right). \quad (17)$$

Note that y in (17) is an independent variable. Therefore, in order to prove (17), we need to show that for every m, the coefficients of $C_{2m}\phi_{tm}(y)$ on the left and right sides of (17) are equal. Thus, we need to prove

$$\frac{2e^{j((2K-2)/8K)\pi}}{\sqrt{2K}} \sum_{q=0}^{K-1} \exp\left(-\frac{jq(q+1)}{2K}\pi\right) \times \cos\left(\frac{(2m+1)(2q+1)\pi}{4K}\right) = \exp\left(\frac{jm(m+1)}{2K}\pi\right) \quad (18)$$

which simplifies to

$$\frac{2e^{j((N-2)/4N)\pi}}{\sqrt{2K}} \sum_{q=0}^{K-1} \exp\left(-j\frac{q(q+1)+m(m+1)}{2K}\pi\right) \times \cos\left(\frac{(2m+1)(2q+1)\pi}{4K}\right) = 1. \quad (19)$$

Let us simplify the left side of (19)

$$\frac{e^{j((K-1)/4K)\pi}}{\sqrt{2K}} \times \left\{ \sum_{q=0}^{K-1} \exp\left(-j\frac{2q(q+1)+2m(m+1)-(2m+1)(2q+1)}{4K}\pi\right) + \exp\left(-j\frac{2q(q+1)+2m(m+1)+(2m+1)(2q+1)}{4K}\pi\right)\right\} \quad (20)$$

which further simplifies to

$$\frac{e^{j(1/4)\pi}}{\sqrt{2K}} \sum_{q=0}^{K-1} \exp\left(-j\frac{(m-q)^2}{2K}\pi\right) + \exp\left(-j\frac{(m+q+1)^2}{2K}\pi\right). \quad (21)$$

Now, note that

$$\sum_{q=0}^{K-1} \exp\left(-j\frac{(m-q)^2}{2K}\pi\right) + \exp\left(-j\frac{(m+q+1)^2}{2K}\pi\right) = \sum_{q=m+1-K}^{m+K} \exp\left(-j\frac{q^2}{2K}\pi\right). \quad (22)$$

Consider a set of integer numbers $\{m-K+1,\ m-K+2, \ldots,\ m+K\}$. Regardless of m, this set modules $2K$ is exactly the same as $\{0,\ 1, \ldots,\ 2K-1\}$mod$(2K)$. It can be easily shown that if $a \equiv b$ mod$(2K)$, then $a^2 \equiv b^2$ mod$(4K)$, hence $\exp(-j2\pi a^2/4K) = \exp(-j2\pi b^2/4K)$ or $\exp(-j\pi a^2/2K) = \exp(-j\pi b^2/2K)$. Therefore, the expression in (19) is independent from m as follows:

$$\sum_{q=m+1-K}^{m+K} \exp\left(-j\frac{q^2}{2K}\pi\right) = \sum_{q=0}^{2K-1} \exp\left(-j\frac{q^2}{2K}\pi\right). \quad (23)$$

From the above-mentioned statements, we can also conclude

$$\sum_{q=0}^{2K-1} \exp\left(-j\frac{q^2}{2K}\pi\right) = \sum_{q=1}^{2K} \exp\left(-j\frac{q^2}{2K}\pi\right) = \sum_{q=2K+1}^{4K} \exp\left(-j\frac{q^2}{2K}\pi\right) \quad (24)$$

which leads to

$$\sum_{q=m+1-K}^{m+K} \exp\left(-j\frac{q^2}{2K}\pi\right) = \frac{1}{2}\sum_{q=1}^{4K} \exp\left(-j\frac{q^2}{2K}\pi\right). \quad (25)$$

Using the reciprocity law for quadratic Gauss, sums defined as

$$G(N;M) = \sum_{q=1}^{M} \exp(j2\pi Nq^2/M) \quad (26)$$

we can write the results as follows:

$$G(N=1,M)=\sum_{q=1}^{M}\exp(j2\pi q^2/M)$$
$$=\frac{1}{2}\sqrt{M}(1+j)(1+e^{-j\pi M/2}) \quad (27)$$

which is equal to $(1+j)\sqrt{M}$ if $M\equiv 0 \bmod(4)$. Comparing (25) and (27), we can conclude

$$\sum_{q=m+1-K}^{m+K}\exp\left(-j\frac{q^2}{2K}\pi\right)=\frac{1}{2}G^*(1,4K)=\frac{1}{2}(1-j)\sqrt{4K}$$
$$=(1-j)\sqrt{K}=\exp\left(-j\frac{\pi}{4}\right)\sqrt{2K} \quad (28)$$

where G^* is the complex conjugate of G. Considering (19), (22), (23), and (28), we can write

$$\frac{2e^{j((N-2)/4N)\pi}}{\sqrt{2K}}\sum_{q=0}^{K-1}\exp\left(-j\frac{q(q+1)+m(m+1)}{2K}\pi\right)$$
$$\times\cos\left(\frac{(2m+1)(2q+1)\pi}{4K}\right)=\frac{e^{j(1/4)\pi}}{\sqrt{2K}}\sum_{q=0}^{2K-1}\exp\left(-j\frac{q^2}{2K}\pi\right)$$
$$=\frac{e^{j(1/4)\pi}}{\sqrt{2K}}\times\exp\left(-j\frac{\pi}{4}\right)\sqrt{2K}=1. \quad (29)$$

Therefore, we have proved (18) and consequently (17).

APPENDIX B
PROOF FOR ODD N

In the case of $N=2K+1$, $K\in\mathbb{Z}$, we need to prove

$$\frac{e^{j((N-1)/4N)\pi}}{\sqrt{N}}\sum_{m=0}^{M/2}C_{2m}\phi_{2m}(y)$$
$$\times\left(1+2\sum_{q=1}^{(N-1)/2}\exp\left(-j\frac{q^2}{N}\pi\right)\cos\left(\frac{2m+1}{N}q\pi\right)\right)$$
$$=\sum_{m=0}^{M/2}C_{2m}\phi_{tm}(y)\exp\left(j\frac{m(m+1)}{N}\pi\right). \quad (30)$$

Similar to the case of even N, since y in (17) is an independent variable, in order to prove (30), we need to show that for every m, the coefficients of $C_{2m}\phi_{tm}(y)$ on the left and right sides of (30) are equal. Thus, we need to prove

$$\frac{e^{j((N-1)/4N)\pi}}{\sqrt{N}}\left(1+2\sum_{q=1}^{(N-1)/2}\exp\left(-j\frac{q^2}{N}\pi\right)\cos\left(\frac{2m+1}{N}q\pi\right)\right)$$
$$=\exp\left(j\frac{m(m+1)}{N}\pi\right) \quad (31)$$

or equivalently

$$\frac{e^{j((2K)/4(2K+1))\pi}}{\sqrt{2K+1}}\left\{\exp\left(-j\frac{m(m+1)}{2K+1}\pi\right)\right.$$
$$\left.+2\sum_{q=1}^{K}\exp\left(-j\frac{q^2+m(m+1)}{2K+1}\pi\right)\cos\left(\frac{2m+1}{2K+1}q\pi\right)\right\}=1. \quad (32)$$

Consider the left-hand side of (32)

$$\frac{e^{j((K)/2(2K+1))\pi}}{\sqrt{2K+1}}\left\{\exp\left(-j\frac{m(m+1)}{2K+1}\pi\right)\right.$$
$$+\sum_{q=1}^{K}\exp\left(-j\frac{q^2+m(m+1)-(2m+1)q}{2K+1}\pi\right)$$
$$\left.+\exp\left(-j\frac{q^2+m(m+1)+(2m+1)q}{2K+1}\pi\right)\right\} \quad (33)$$

which simplifies to

$$\frac{e^{j((K)/2(2K+1))\pi}}{\sqrt{2K+1}}\left\{\exp\left(-j\frac{m(m+1)}{2K+1}\pi\right)\right.$$
$$+\sum_{q=1}^{K}\exp\left(-j\frac{(q-m-1/2)^2-1/4}{2K+1}\pi\right)$$
$$\left.+\exp\left(-j\frac{(q+m+1/2)^2-1/4}{2K+1}\pi\right)\right\} \quad (34)$$

and further simplifies to

$$\frac{e^{j(\pi/4)}}{\sqrt{2K+1}}\left\{\exp\left(-j\frac{(m+1/2)^2}{2K+1}\pi\right)\right.$$
$$+\sum_{q=1}^{K}\exp\left(-j\frac{(q-m-1/2)^2}{2K+1}\pi\right)$$
$$\left.+\exp\left(-j\frac{(q+m+1/2)^2}{2K+1}\pi\right)\right\}. \quad (35)$$

Note that

$$\exp\left(-j\frac{(m+1/2)^2}{2K+1}\pi\right)+\sum_{q=1}^{K}\left\{\exp\left(-j\frac{(q-m-1/2)^2}{2K+1}\pi\right)\right.$$
$$\left.+\exp\left(-j\frac{(q+m+1/2)^2}{2K+1}\pi\right\}\right)$$
$$=\sum_{q=-K}^{K}\exp\left(-j\frac{(2q+2m+1)^2}{4(2K+1)}\pi\right). \quad (36)$$

Consider $q=n(2K+1)+r$, $-K\le q\le K$ and $0\le r\le 2K$. Then, $\{q+m\}\bmod(2K+1)\equiv\{q\}\bmod(2K+1)$ with the same set of residuals $\{r\}$, for every integer m. In addition,

$\{2m+2q+1\} \bmod (2K+1)$ is the set of $\{2r+1\}$. Therefore, $\forall m \in \mathbb{Z}$ and $\forall q \in \{q\}$, $\exists r \in \{q\}$ so that $2m+2q+1 = 2p(2K+1)+(2r+1)$ for some integer p. We can write

$$(2m+2q+1)^2 = 4p(2K+1)[p(2K+1) + (2r+1)] + (2r+1)^2. \quad (37)$$

Also note that $p\,[p(2K+1)+(2r+1)]$ is always even. Thus, $(2m+2q+1)^2 = 8s(2K+1)+(2r+1)^2$, for some integer s, and

$$\sum_{q=-K}^{K} \exp\left(-j\frac{(2q+2m+1)^2}{4(2K+1)}\pi\right) = \sum_{r=0}^{2K} \exp\left(-j\frac{(2r+1)^2}{4(2K+1)}\pi\right) = \exp\frac{-j\pi}{4(2K+1)} \sum_{r=0}^{2K} \exp\frac{r^2+r}{2K+1}\pi. \quad (38)$$

Now consider the Gauss quadratic reciprocity law, $\forall a, b, c, z \in \mathbb{Z}$, $ac \neq 0$ and $ac+b$ even

$$\sum_{z=0}^{|c|-1} \exp\left(j\pi\frac{az^2+bz}{c}\right) = \sqrt{|c/a|}\exp\left(j\pi\frac{|ac|-b^2}{4ac}\right) \sum_{z=0}^{|a|-1} \exp\left(j\pi\frac{cz^2+bz}{a}\right). \quad (39)$$

Let $a, b = 1$, $z = r$, and $c = 2K+1$, we can see that $ac+b = 2K+2$ is even, therefore, we can use the Gauss quadratic reciprocity law

$$\exp\frac{-j\pi}{4(2K+1)} \sum_{r=0}^{2K} \exp\frac{r^2+r}{2K+1}\pi = \exp\frac{-j\pi}{4(2K+1)} \times \sqrt{2K+1}\exp\left(-j\pi\frac{2K}{4(2K+1)}\right) = \sqrt{2K+1}\exp -j\frac{\pi}{4}. \quad (40)$$

From (35) and (40)

$$\frac{e^{j(\pi/4)}}{\sqrt{2K+1}}\left\{\exp\left(-j\frac{(m+1/2)^2}{2K+1}\pi\right) + \sum_{q=1}^{K}\exp\left(-j\frac{(q-m-1/2)^2}{2K+1}\pi\right) + \exp\left(-j\frac{(q+m+1/2)^2}{2K+1}\pi\right)\right\} = \frac{e^{j(\pi/4)}}{\sqrt{2K+1}} \times \sqrt{2K+1}\exp\left(-j\frac{\pi}{4}\right) = 1. \quad (41)$$

Therefore, we have proved (31) and consequently (30).

ACKNOWLEDGMENT

The authors would like to thank Dr. A. Keshavarz-Haddad from the Department of Electrical and Computer Engineering, Rice University, Houston, TX, Prof. F. R. Villegas, and Prof. F. Voloch from the Department of Mathematics, University of Texas at Austin, Austin, TX, for the helpful discussions and comments.

REFERENCES

[1] J. S. Yu, J. Y. Moon, S. M. Choi, and Y. T. Lee, "Fabrication of 1×8 multimode-interference optical power splitter based on InP using CH_4/H_2 reactive ion etching," *Jpn. J. Appl. Phys.*, vol. 40, no. 2A, pp. 634–639, 2001.

[2] X. Wang and R. T. Chen, "Image enhanced polymer-based multimode interference coupler covering C and L bands using deeply etched air trenches," *Appl. Phys. Lett.*, vol. 90, no. 11, pp. 111106-1–111106-3, 2007.

[3] L. Soldano and E. Pennings, "Optical multi-mode interference devices based on self-imaging: Principles and applications," *J. Lightw. Technol.*, vol. 13, no. 4, pp. 615–627, Apr. 1995.

[4] X. Chen, W. Jiang, J. Chen, L. Gu, and R. T. Chen, "20 db-enhanced coupling to slot photonic crystal waveguide using multimode interference coupler," *Appl. Phys. Lett.*, vol. 91, no. 9, pp. 091111-1–091111-3, 2007.

[5] Y.-J. Chang, T. K. Gaylord, and G.-K. Chang, "Pulse response of multimode interference devices," *J. Lightw. Technol.*, vol. 24, no. 3, pp. 1462–1469, Mar. 2006.

[6] J. Xia, J. Yu, Z. Wang, Z. Fan, and S. Chen, "Low power 2×2 thermo-optic SOI waveguide switch fabricated by anisotropy chemical etching," *Opt. Commun.*, vol. 232, no. 1–6, pp. 223–228, 2004.

[7] M. Paiam and R. MacDonald, "A 12-channel phased-array wavelength multiplexer with multimode interference couplers," *IEEE Photon. Technol. Lett.*, vol. 10, no. 2, pp. 241–243, Feb. 1998.

[8] M. Rajarajan, B. Rahman, T. Wongcharoen, and K. Grattan, "Accurate analysis of MMI devices with two-dimensional confinement," *J. Lightw. Technol.*, vol. 14, no. 9, pp. 2078–2084, Sep. 1996.

[9] J. Huang, R. Scarmozzino, and R. M. Osgood, Jr, "A new design approach to large input/output number multimode interference couplers and its application to low-crosstalk WDM routers," *IEEE Photon. Technol. Lett.*, vol. 10, no. 9, pp. 1292–1294, Sep. 1998.

[10] R. Ulrich and T. Kamiya, "Resolution of self-images in planar optical waveguides," *J. Opt. Soc. Amer.*, vol. 68, no. 5, pp. 583–592, 1978.

[11] R. M. Lorenzo, C. Llorente, and E. J. A. M. Lopez, "Improved self-imaging characteristics in i x n multimode couplers," *Inst. Electr. Eng. Proc.-Oproelectron.*, vol. 145, no. 1, pp. 65–69, Feb. 1998.

[12] R. Yin, X. Jiang, J. Yang, and M. Wang, "Structure with improved self-imaging in its graded-index multimode interference region," *J. Opt. Soc. Amer. B*, vol. 19, no. 6, pp. 1301–1303, 2002.

[13] M. Jarrahi, R. F. W. Pease, D. A. B. Miller, and T. H. Lee, "Optical switching based on high-speed phased array optical beam steering," *Appl. Phys. Lett.*, vol. 92, no. 1, pp. 014106-1–014106-3, 2008.

[14] M. Bachmann, P. A. Besse, and H. Melchior, "General self-imaging properties in $N \times N$ multimode interference couplers including phase relations," *Appl. Opt.*, vol. 33, no. 18, pp. 3905–3911, 1994.

[15] M. Jarrahi, R. F. W. Pease, and T. H. Lee, "Spatial quantized analog-to-digital conversion based on optical beam-steering," *J. Lightw. Technol.*, vol. 26, no. 14, pp. 2219–2226, Jul. 2008.

[16] S. Nakamura, Y. Ueda, S. Fujimoto, H. Yamada, and K. Utaka, "Versatile optical switching of 44 novel slotted multi-mode interference phase-arrayed photonic switch," in *Proc. Int. Nano-Optoelectron. Workshop (i-NOW 2008)*, pp. 343–344.

[17] T. Rasmussen, J. Rasmussen, and J. Povlsen, "Design and performance evaluation of 1-by-64 multimode interference power splitter for optical communications," *J. Lightw. Technol.*, vol. 13, no. 10, pp. 2069–2074, Oct. 1995.

[18] T. F. Jablonski, "Complex modes in open lossless dielectric waveguides," *J. Opt. Soc. Amer. A*, vol. 11, no. 4, pp. 1272–1282, 1994.

[19] P.-L. Liu, S. Yang, and D. Yuan, "The semivectorial beam propagation method," *IEEE J. Quantum Electron.*, vol. 29, no. 4, pp. 1205–1211, Apr. 1993.

Amir Hosseini (S'05) received the B.Sc. degree (Hons.) in electrical engineering from Sharif University of Technology, Tehran, Iran, in 2005, and the M.S. degree in electrical and computer engineering from Rice University, Houston, TX, in 2007. He is currently working toward the Ph.D. degree in the Department of Electrical and Computer Engineering, Microelectronics Research Center, University of Texas at Austin, Austin, TX with Dr. R. T. Chen's Optical Interconnect Group, where he has been engaged in research on optical phased array technology and high performance optical modulators design and optimizations.

His current research interests include the design optimization for nanoscale manufacturability.

David Kwong received the B.S. degree in electrical engineering from the University of Texas at Austin, Austin, TX, in 2006. He is currently working toward the Master's degree in the Department of Electrical and Computer Engineering, Microelectronics Research Center, University of Texas at Austin, Austin, TX with the Optical Interconnect Group, where he has been engaged in optical phased array technology and optical modulation.

He was at Samsung Austin Semiconductor in process integration for dynamic random-access memory back end of line processes for two years, before joining the University of Texas at Austin.

Che-Yun Lin (S'09) received the B.S. degree in electronic engineering from Chang Gung University, Taoyuan, Taiwan, in 2006, and the M.S.E. degree in electrical and systems engineering from the University of Pennsylvania, Philadelphia, PA, in 2008. He is currently working toward the Ph.D. degree in the Department of Electrical and Computer Engineering, Microelectronics Research Center, University of Texas at Austin, Austin, TX with Prof. Ray T. Chen's Optical Interconnect Group, where is engaged in design, fabrication, and characterization of microwave and silicon photonics devices.

His current research includes experimental demonstration of miniaturized high-speed silicon photonic crystal modulator.

Beom Suk Lee received the B.Sc. and the M.S. degrees in material science and engineering from Seoul National University, Seoul, Korea, in 1999 and 2001, respectively. He is currently working toward the Ph.D. degree in the Department of Electrical and Computer Engineering, Microelectronics Research Center, University of Texas at Austin, Austin, TX with Dr. R. T. Chen's Optical Interconnect Group, where he has been engaged in research on high performance optical modulators based on electro-optic polymer incorporated in silicon and polymer platforms.

His current research interest includes the optimization of device fabrication and characterization.

Ray T. Chen (M'91–SM'98–F'04) received the B.S. degree in physics from National Tsing-Hua University, Hsinchu, Taiwan, in 1980, the M.S. degree in physics, and the Ph.D. degree in electrical engineering from University of California, LA, in 1983 and 1988, respectively.

From 1988 to 1992, he was a Research Scientist, Manager, and Director in the Department of Electrooptic Engineering, Physical Optics Corporation, Torrance, CA. Since 1992, he is a Faculty Member in the Department of Electrical and Computer Engineering, Microelectronics Research Center, University of Texas at Austin, Austin, TX, where he has been engaged in the optical interconnect research program. From 2000 to 2001, he was Chief Technology Officer/Founder and Chairman of the Board of Radiant Research, where he raised 18 million dollars A-Round funding to commercialize polymer-based photonic devices. He also serves as the founder and Chairman of the Board of Omega Optics Inc., since its initiation in 2001, where more than 5 million dollars of research funds were raised. He holds the Cullen Trust for Higher Education Endowed Professorship at University of Texas at Austin and the Director of nanophotonics and optical interconnects research laboratory within the microelectronics research center. He is also the Director of a newly formed Air Force Office of Scientific Multidisciplinary Research Initiative Center for Silicon Nanomembrane involving faculty from Stanford, University of Illinois at Urbana-Champaign, Rutgers, and University of Texas at Austin. His research interest includes nanophotonic passive and active devices for optical interconnect applications, polymer-based guided-wave optical interconnection and packaging, and True time delay wide band phased array antenna. Experiences garnered through these programs in polymeric material processing and device integration are pivotal elements for the research work conducted by Chen's group. Chen's group has published more than 510 articles and 80 invited papers. He holds 18 issued patents. He has chaired or been a program-committee member for more than 90 domestic and international conferences organized by IEEE, The International Society of Optical Engineering (SPIE), Optical Society of America (OSA), and The Physics Society of Chinese Americans. He has served as an editor, co-editor or coauthor for 22 books. He also served as a consultant for various federal agencies and private companies and delivered numerous invited talks to professional societies. There are 32 students who received the electrical engineering Ph.D. degree in Chen's research group at University of Texas at Austin.

Dr. Chen is a Fellow of OSA and SPIE. He was the recipient 1987 University of California Regent's Dissertation Fellowship and of 1999 University of Texas Engineering Foundation Faculty Award for his contributions in research, teaching and services. His research work has been awarded with 94 research grants and contracts from sponsors such as DOD, NSF, DOE, NASA, the State of Texas, and private industry. Back to his undergraduate years in National Tsing-Hua University, he led a university debate team in 1979, which received the National Championship of National Debate Contest in Taiwan.